SACLANTCEN REPORT
serial no: SR-306

SACLANT UNDERSEA RESEARCH CENTRE REPORT

A NEURAL-NETWORK-FUSION ARCHITECTURE FOR AUTOMATIC EXTRACTION OF OCEANOGRAPHIC FEATURES FROM SATELLITE REMOTE SENSING IMAGERY

F. Askari, B. Zerr

June 1999

SACLANT Undersea Research Centre
Viale San Bartolomeo 400
19138 San Bartolomeo (SP), Italy

tel: +39-0187-5271
fax: +39-0187-524.600

e-mail: library@saclantc.nato.int

NORTH ATLANTIC TREATY ORGANIZATION

Report no. changed (Mar 2006): SR-306-UU

A neural-network-fusion architecture for automatic extraction of oceanographic features from satellite remote sensing imagery.

Farid Askari and Benoit Zerr

The content of this document pertains to work performed under Project 014-1 of the SACLANTCEN Programme of Work. The document has been approved for release by The Director, SACLANTCEN.

Jan L. Spoelstra
Director

intentionally blank page

A neural-network-fusion architecture for automatic extraction of oceanographic features from satellite remote sensing imagery.

Farid Askari and Benoit Zerr

Executive Summary: Satellite remote sensing imagery provides the ASW/MW operational community with a synoptic view of the prevailing environmental conditions and the capability to extract information on oceanic features/processes affecting acoustic propagation conditions. The high data volumes and throughputs generated by earth observing satellites call for the implementation of advanced information systems including automatic pattern recognition that can aid the analyst in filtering, synthesizing, monitoring fast changing environments, and locating high-interest targets and features more efficiently. The work reported here focuses on automatic detection of oceanographic features in satellite imagery, using artificial intelligence techniques. The proposed architecture lays the foundation for multi-sensor data fusion and extraction of information for rapid environmental assessment (REA) applications. Future work involves the expansion of the number of signatures and decision rules in the knowledge bank for a more complete representation and classification of tactically relevant features in satellite imagery.

intentionally blank page

A neural-network-fusion architecture for automatic extraction of oceanographic features from satellite remote sensing imagery.

Farid Askari and Benoit Zerr

Abstract: This report describes an approach for automatic feature detection from fusion of remote sensing imagery using a combination of neural network architecture and the Dempster-Shafer (DS) theory of evidence. Deterministic or idealized shapes are used to characterize surface signatures of oceanic and atmospheric fronts manifested in satellite remote sensing imagery. Raw satellite images are processed by a bank of radial basis function (RBF) neural networks trained on idealized shapes. The final classification results from the fusion of the outputs of the separate RBF. The fusion mechanism is based on DS evidential reasoning theory. The approach is initially tested for detecting different features on a single sensor and extended to classifying features observed by multiple sensors.

Keywords: automatic detection, remote sensing, neural networks, sensor fusion.

Contents

1 Introduction

Today, the remote sensing community is faced with two critical problems. First is the problem of the management of high data volumes generated by the earth-observing satellites, and second is, the integration of multiparameter measurements from different satellites and sensors. On both fronts the magnitudes of the problems are expected to grow at an accelerated pace. By the end of the decade there will be a dozen dedicated ocean monitoring satellites in orbit equipped with advanced sensors which are capable of recording several hundred spectral and polarimetric channels simultaneously over a single resolution cell and with data rates of over 100 Mbps. As such a phenomenon on the ocean surface may produce numerous different sets of responses from different sensors. There is therefore a pressing need for more advanced information systems which in addition to high-speed networking systems and high processing capacity incorporate intelligent and automatic pattern recognition. New quantitative decision making tools must be developed for fusing and assimilating large volume multidimensional data into usable products. Hence, the objectives of the research presented in this paper are twofold: 1) Develop a methodology for automatic oceanographic feature detection and extraction in satellite remote sensing imagery, 2) Develop a system architecture for information and sensor fusion. The role of automatic pattern recognition and feature extraction systems is to assist the resource analyst in filtering and synthesizing vast volumes of data more rapidly, optimizing decisions, and monitoring fast changing environments more quickly.

Much published material exists on the general problems of automatic pattern recognition, feature extraction, and combining multiple classifiers. For automatic pattern recognition several classification algorithms are available including the Baysian classifier, k-nearest neighbor (k-NN), distance classifiers [1] and a family of neural-network (NNT) based classifiers [2]. Feature extraction schemes make use of spatial information and shape descriptors for detection and classification. The distinctive characteristics of each feature may be derived from Fourier descriptors, moments, texture analysis, the Hough transform [3] and the two-dimensional wavelet transform [4]. For improving the overall classification accuracy or increasing the efficiency of the system, several schemes are used for combining classifiers [5,6] including majority voting, sum rule, product rule, fuzzy integral [7], and the Dempster-Shafer (DS) formalism [8,9]. The primary focus of the studies cited above, however, has been on speech, handwriting and character recognition applications. With the exception of the wavelet transform [4], little has been published on the applications of such techniques to satellite oceanography.

Our work introduces a new approach to automatic feature detection and sensor fusion in remote sensing imagery which relies on a combination of neural network architecture and the DS theory of evidence. The use of neural networks for classification purposes is of course not new. The approach reported here, however, differs from previous investigations. Most investigations using neural-networks for classification rely solely on the outputs of the networks as the discriminator. That is, after the network is trained and a generalized relationship between input-output is derived, new data is classified as belonging to a certain class by choosing the maximum network output. Here, the network outputs are used as inputs to a classifier, which uses the information in the framework of DS formalism to arrive at classification results. In other words the neural network outputs are treated as *posteriori* probabilities, with each network supplying independent evidence to the classifier. Our approach also provides for more flexibility in fusing information from multi-source images when the sensors have different spatial resolutions. Each image is classified independently and the final classification results are transferred to a geographic map in the form of symbols or contours. Moreover our approach differs from traditional image processing schemes in the manner in which 2-D information is processed. Here, we use a template consisting of four 1-D profiles taken at different orientations over the image. As such, the classification system is capable of dealing with shape information and features containing 2-D spatial variability, without complex and time consuming processing such as 2-D texture analysis.

The article is organized as follows. In Section 2, we show the various types of signatures for the oceanographic features and the rational for selecting the shape-kernels which form the basis for automatic detection. We then formulate the neural network and fusion architectures. The results of applying the technique to image classification and feature detection are shown in Section 3. It is shown that the system is capable of detecting oceanic frontal features in satellite imagery on the basis of training on idealized shapes. Using sensor fusion and a set of predefined rules we develop a methodology for discriminating between wind-induced versus sea surface temperatude-induced roughness fronts. Also a strategy for automatic detection of salinity fronts is proposed by fusing signatures from the roughness and color fields. The conclusions are given in Section 4. The approach presented is well suited to rapid, accurate and systematic search of features in a single image or multi-sensor data.

2
Materials and Methods

This section describes the overall automatic detection system. First, we show examples of oceanographic features and their corresponding signatures that provide the basis for the automatic detection problem. Descriptions of the neural network and fusion architectures and a demonstration of the technique in classifying idealized patterns and features follow.

2.1 Oceanographic Features and Signatures

When interpreting satellite imagery, the human eye uses a combination of tonal, spatial structures and textural features as visual indicators for recognizing or distinguishing features from their backgrounds. In order for a machine to learn and recognize features automatically, low-level and high-level information must be furnished to the pattern recognition system. The low-level information consists of feature attributes such as edges or intensity changes, lines or regions. The high-level information consist of knowledge representations and inference mechanisms which describe the feature's physical attributes. Tonal or intensity modulations as well as the shapes are utilized as the basic low-level information for feature extraction. Modulation is defined as the change in local image intensity with respect to the mean background intensity.

In describing high-level information, knowledge can be represented as declarative or procedural [10]. In declarative representation, knowledge is assembled through historical evidence. In procedural representation a set of predefined rules govern the flow of information and decisions. The following discussion and examples illustrate the manner in which we utilize declarative knowledge in formulating the pattern recognition system. Numerous studies have reported the relationships between intensity modulations in the roughness, color and the temperature fields to physical processes on the ocean. Among processes contributing to variations in the water "color" in coastal regions are river discharge of dissolved organic matter and suspended sediment, re-suspension of bottom material due to tidal currents, storms and wave action, algal blooms and nutrient loading [11]. For small-scale roughness, the primary geophysical processes that modulate the backscattered radar cross-section are temperature fronts, discontinuities in the wind field, interactions between long-waves and short-waves, interactions between waves and currents and surfactants and surface films [12]. Processes contributing to sea surface temperature anomalies include diurnal heating and cooling, upwelling, diffusion or advection by currents, filaments and eddies [13].

Consider the variations in sea surface roughness as shown in an ERS-2 SAR image (Fig. 1). The 1-D vertical profile (Fig. 1b) across feature A shows a distinct step-like (bright-to-dark) change in surface roughness with a smoother surface on the upper portion of the image. Historical evidence suggests that in SAR imagery, two primary physical mechanisms contribute to step-like changes in sea surface roughness [14, 15]: wind stress changes induced by the thermal stability variations near a SST front and wind stress changes induced by an impulsive atmospheric wind/gust front [16]. Examples of similar features and patterns appear in [16]. A 1-D horizontal profile across feature B (Fig. 1c) shows a bright signature with enhanced roughness concentrated over a narrow region. It is widely accepted that narrow-banded modulations are associated with regions of strong wave current interactions, ie, convergent fronts [16], when the modulation is positive (bright) and with the accumulation of surfactants, when modulations are negative (dark) [12].

In a declarative knowledge base containing step-like and Gaussian-shaped features the modulations are as follows. For a step-like feature a distinct boundary separates two regions with different mean image intensities, whereas for the Gaussian-shaped feature, a pulse of finite width stands above or below a mean background. The idealized shapes provide an adequate description of certain types of oceanic fronts in remote sensing imagery. The first type is often associated with boundaries of large-scale currents and eddies observed in advanced very high resolution (AVHRR) or Sea-viewing Wide Field-of-view Sensor (SeaWIFS) imagery, and wind and sea surface temperature (SST) fronts in SAR imagery. And the second type is often associated with river and estuarine plumes, current filaments and jets in AVHRR or SeaWIFS imagery and velocity fronts and slicks in SAR imagery. To further generalize the problem and account for the various sensor resolutions, feature length-scales and sensor look-angle dependencies, we construct pattern/feature functions with a broad range of adjustable parameter. The step-like modulations are further divided into two subclasses: steps with intensities increasing from left-to-right, and steps with intensities decreasing from right-to-left. In addition to the vertical steps, the steps are permitted to contain ramps with varying slopes. For the Gaussian-shaped pulses, which can be either positive or negative, the pulse widths are varied (Fig. 2).

Recent research has shown that many ocean features produce anomalous signatures in more than one field. Sometimes a surface feature may produce signature anomalies in all three fields, while in others only two of the fields may be expressed. When the fields do appear concurrently the question is whether the fields are collocated or is there horizontal dislocation. There are situations for example with roughness and SST fronts, where one field can lag or lead the other depending on the structure of the atmospheric boundary layer or the wind direction [14]. It is also likely that when observing a frontal system, anomalous signals may emerge from different positions within the front because of the differences in the penetration depths of the electromagnetic waves into the surface. The IR and microwave energies are due to surface processes, whereas the color field results from light upwelled from below the surface.

The ultimate goal of fusion of the various sensors and features is, however, to arrive at a knowledge base that has a higher information content than the individual parts. Next, we demonstrate how the shapes can be incorporated in a neural network for automatic feature detection.

2.2 Neural network architecture

Artificial neural networks are well suited to a variety of problems in signal and image processing in which competing hypotheses are pursued simultaneously and rapidly [2]. The behavior and practical characteristics in terms of error rates, training time, classification time, and memory requirement of several different networks and classifiers are compared in [17]. A review of neural networks for classification of multi-spectral remotely sensed imagery is given in [18].

The neural network architecture used here relies on radial basis functions (RBF) [2, 19] for training and pattern classification. The RBF network belongs to the family of multilayer feedforward neural networks. In network design, one of the important considerations in choosing the classifiers is how the classifier partitions the feature-space and the shapes of its decision boundaries. How well a classifier can generalize and discriminate, new unseen data depends on the structure of its decision regions. The RBF classifiers have relatively smooth decision boundaries, and are thus able to generalize well to unseen data [17].

The neural network (Fig. 3) used here consists of three layers: input layer containing the input nodes, hidden layer containing the basis function (BF) nodes, and the output layer containing the output nodes. In general, a network is trained or tuned to recognize patterns by being shown a given set of input-output pairs. The tunable parameters take the form of weights.

The first step in training involves the specification of the number of basis functions (BF). For our particular problem we determined that five BF are sufficient to achieve the desired classification performance. Unit weights connect the input layer to the second layer.

The second layer consists of a number of multi-dimensional Gaussian BF defined by:

$$y_j = \sum_{i=1}^{n} w_{ij} \exp\left(-\frac{1}{2\sigma_i^2} \| X - C_i \|^2 \right) + b_j \qquad (2.1)$$

where $X = (x_1, x_2, ... x_p)$ is the input vector, and $Y = (y_1, y_2, ... y_p)$ is the output vector, C_i is mean vector and σ_i is the covariance matrix, n is the number of BF, and b_j is a bias term which is used to threshold the output of the jth neuron in the output layer. The second step in training involves determining the BF centers and variances or widths of the BF. The RBF classifier is essentially a function mapping interpolation method that partitions the n-dimensional measurement space into hyper-volumes or regions belonging to the separate classes. The RBF centers and widths define the hyper-volumes. The mean vectors are computed from the training set by a fuzzy c-means clustering algorithm [19], where the number of clusters are equal to the number of BF needed by the network. The variance is computed using the nearest four neighbors.

The output nodes z_j are activated using a linear combination of the BF nodes:

$$z_j = \sum_i w_{ij} y_i + w_{0j} \tag{2.2}$$

where z_j is the output of the jth output node, y_i is the activation of the ith BF node and w_{ij} is the weight connecting the ith BF node to the jth output node, and w_{0j} is the bias of the jth output node. The third step of the training process involves computing the weights, which are determined using matrix pseudo-inverse approach. When classification is exclusively performed by RBF, an input vector is classified as belonging to the class associated with the output node with the largest response.

2.3 *Fusion Mechanism*

In the previous section we described the architectural details of the neural network. For many applications it is standard practice to use the network as a stand-alone classifier and choose the maximum output from a given node for selecting a particular class. Our goal here, however, is to extend the technique into a classification strategy for multiple information/sensor fusion.

We first show the application of the technique for detecting features in a single image/sensor. A 2-D image is classified using four 1-D profiles. For each 1-D profile, the network outputs an independent decision or belief that the detected profile belongs to one of the predefined classes. The individual opinions are then fused to derive the final classification results. The fusion mechanism is based on the DS theory of evidential reasoning [9, 21]. The DS theory is a mathematical formalism for assigning beliefs to a set of hypothesis, and for combining belief in a consistent manner. First, we illustrate the DS techniques by a simple numerical example, and later show graphically the behavior the network/classifier using idealized features.

The principal requirement for the application of the DS is the construction of the frame of discernment (FOD). The elements of the FOD are chosen as the possible features that might be encountered on a satellite image. We define the FOD by the set $\theta = \{F1, F2\}$, where F1 and F2 are two separate features. Contrary to a probability

distribution, which assigns belief to the elements of FOD, the DS theory assigns belief to all possible subsets of the FOD, and actually distinguishes between uncertainty and ignorance. The degree of ignorance is introduced by assigning belief to the whole frame of θ. Here, we use the RBF outputs for assigning belief.

For demonstration we extract a vertical and a horizontal profile over two hypothetical features. The RBF is trained to distinguish between the two features using only two elementary profiles, p1 and p2. The output of the RBFs for the vertical and horizontal profiles respectively, are $\{p1_v, p2_v\}$, and $\{p1_h, p2_h\}$. We assume that F1 and F2 are isotropic features, such that the evidence from the horizontal and vertical profiles can be combined directly. The possible subsets of FOD are {F1}, {F2}, {F1, F2}, and {θ}.

Now suppose that the RBF outputs result in the following set of beliefs: $p1_v = 0.8$, $p2_v = 0.2$, $p1_h = 0.55$, $p2_h = 0.45$. Here both belief functions, ($p1_v > p2_v$) and ($p1_h > p2_h$), support the hypothesis that feature F1 is present, although the support from the horizontal profile is weaker than the vertical profile. Now if we submit the following set of beliefs:

$$m_1(\{\theta\}) = 1\text{-}p1_v = a_v = 0.2 \quad (2.3)$$
$$m_1(\{F1\}) = p1_v\text{-}p2_v = b_v = 0.6 \quad (2.4)$$
$$m_1(\{F1,F2\}) = p2_v = c_v = 0.2 \quad (2.5)$$

and,

$$m_2(\{\theta\}) = 1 - p1_h = a_h = 0.45 \quad (2.6)$$
$$m_2(\{F1\}) = p1_h - p2_h = b_h = 0.1 \quad (2.7)$$
$$m_2(\{F1,F2\}) = p2_h = c_h = 0.45 \quad (2.8)$$

to the DS and use the orthogonal sum ($m = m_1 \oplus m_2$) combination rule [21]:

$$m(A) = \frac{\sum_{B\cap C=A} m_1(B)\ m_2(C)}{1-\sum_{B\cap C=0} m_1(B)\ m_2(C)} \quad (2.9)$$

provided that

$$\sum_{B\cap C=0} m_1(B)\ m_2(C) < 1. \quad (2.10)$$

The order in which mass functions are combined is irrelevant because the orthogonal sum is commutative, $m_1 \oplus m_2 = m_2 \oplus m_1$, and associative, $m_1 \oplus (m_2 \oplus m_3) = (m_1 \oplus m_2) \oplus m_3$. Using 2.3-2.8 in 2.9 we obtain

$$m(\{F1\}) = m_1(\{\theta\})m_2(\{F1\})+m_2(\{\theta\})m_1(\{F1\})+m_1(\{F1\})m_2(\{F1\})+..$$

$$m_1(\{F1\})m_2(\{F1,F2\})+m_1(\{F1,F2\})m_2(\{F1\}) \quad (2.11)$$

or

$$m(\{F1\}) = a_v\, b_h + a_h\, b_v + b_v\, b_h + b_v\, c_h + c_v\, b_h = 0.64 \quad (2.12)$$

$$m(\{F2\}) = 0.0 \quad (2.13)$$

We obtain a much stronger support for feature F1, using the combined beliefs (m {F1}=0.6, m {F2}=0.0. In this situation, DS concentrates support when there is consent between beliefs and reduces it when there is not. Next we consider a situation of conflict (($p1_v > p2_v$) and ($p1_h < p2_h$), ie, when the beliefs don't agree:

$$m_1(\{\theta\}) = 1\text{-}p1_v = a_v \quad (2.14)$$

$$m_1(\{F1\}) = p1_v\text{-}p2_v = b_v \quad (2.15)$$

$$m_1(\{F1,F2\}) = p2_v = c_v \quad (2.16)$$

and,

$$m_2(\{\theta\}) = 1\text{-}p2_h = a_h \quad (2.17)$$

$$m_2(\{F2\}) = p2_h\text{-}p1_h = b_h \quad (2.18)$$

$$m_2(\{F1,F2\}) = p1_h = c_h \quad (2.19)$$

Combing the above beliefs into DS and using ($m = m_1 \oplus m_2$) we obtain:

$$m(\{F1\}) = (b_v\, a_h + b_v\, c_h)/(1- b_v\, b_h) = 0.574 \quad (2.20)$$

$$m(\{F2\}) = (a_v\, b_h + c_v\, b_h)/(1- b_v\, b_h) = 0.043 \quad (2.21)$$

Here the conflict results in the reduction of support for both hypothesis.

2.4 Pattern Classification Using Idealized Features

Now we apply the technique to a uniform intensity image containing two idealized features, a narrow pulse and a square with intensities different from the background (Fig. 4). The 2-D image is processed by sub-dividing it into a series of square blocks. A template containing four 1-D profiles is used for extracting intensity values along the 0° to 180°, 90° to 270°, 45° to 225°, and 135° to 315° directions. In every block, the intensity values for each profile are processed through a bank of RBFs. The network outputs, which are regarded as a posteriori probabilities are transformed into beliefs belonging to the element of the FOD:

{PULSE, STEP_LH_H, STEP_LH_V, STEP_LH_D1 , STEP_LH_D2,
STEP_HL_H, STEP_HL_V, STEP_HL_D1, STEP_HL_D2}

Where the following notation applies:

LH: low-high transition,
HL: high-low transition,
H: horizontal profile (0-180),
V: vertical profile (90-270),
D1: main diagonal (45-225),
D2: second diagonal (135-315),
PULSE: used the Gaussion profiles for the 4 profiles equivalently.

STEP_LH_H: uses mainly the low-high step from the horizontal profile but also the low-high step from main and second diagonals.
STEP_XX_X are defined in the same way.

Figures 5-8 show the system response when the template is placed in different positions within the 2-D image. The network output consists of a 3x4 matrix, where the first dimension corresponds to feature types (STEP_LH, STEP_HL, Pulse), and the second dimension is the profile orientation (H, V, D1, D2). Figures 5 and 6 illustrate the network response when the template is aligned respectively, with the square's horizontal and vertical edges. When positioned along the vertical edge, the network shows consent between the H and D1-profiles, disagreement between the H or D1 with the D2 profile, and no opinion is given by the V-profile. On the other hand when the template is placed along the horizontal edge, there is consensus among the V, D1, and D2 profiles, and no opinion is given by the H-profile. In the final analysis, in both cases the combined evidence supports the proposition that a step-like feature resides at the location.

Next we consider the case where the template is placed on the pulse, and align D1 parallel to the pulse's main axis. Here, the network response (Fig. 7) shows consent among the H, V, and D2 profiles, with the D1 profile providing no opinion. The combined vote is in favor of the pulse (Fig 7c). Finally, we place the template over a region of uniform intensity (Fig. 8). Here all four profiles respond unanimously to the background noise, and no strong preference is given to either the pulse or to the step. These examples clearly show that a numerical description derived from one or even two profiles is not adequate for classification, but the fusion of information from four profiles do provide sufficient discriminatory power for classifying features with 2-D variability.

3 Results

In this section we first demonstrate the automatic detection/classification capabilities of the system using individual images, and then show the multi-sensor fusion results. For testing the automatic classification three types of satellite imagery are considered: SAR/ERS2 image, AVHRR/NOAA-14 image, and SeaWIFS/ORBVIEW-2.

In the classification stage, the pattern recognition system replaces the visual interpretation step with quantitative decision making. The outputs from the classifiers are essentially thematic maps, in which the pixels in the original imagery are classified into one of the several classes (or themes). The classes in this case are the predefined shapes (steps, pulses) and the outputs correspond to the probability of finding a class at that pixel location. The (0,1) interval in each image is mapped into to the grey scale.

We next present the individual classification results. The SAR image (Fig. 9a) shows two dominant plateau regions where mean intensities (or roughness) change by about 1.6 dB in a step-like fashion. Also visible, are two prominent narrow-bright-curvilinear structures oriented northwest to southeast within the low-roughness region in the northern half of the image. These pulse-shaped features have modulation amplitudes of 1 and 1.6 dB. Figures 9b and 9c show respectively, the classification results when the SAR image is processed through the pattern recognition network for detection of steps, and Gaussian-shaped pulses. In addition to detecting the primary step that separated the plateau regions, the network detected (Fig. 9b) several secondary steps in the lower half of the image, although the amplitudes of these steps are much smaller than the main step. Concerning the detection of pulses, the network was able to identify the curvilinear structures, but in addition, it recognized numerous bright points not easily visible in the original image (Fig. 9c).

Figures 10a-c and show respectively the SAR, AVHRR and SeaWIFS imagery. The SST field shows (Fig. 10b) a distinct front separating cooler (by 1 to 1.5 C^0) coastal water from waters offshore. The SeaWIFS image (Fig. 10c) intensities shown here correspond to variations in k_{532}^{-1}, where k_{532} is the attenuation coefficient for green light. The important observation is the horizontal variability of the k_{532}^{-1} parameter which shows several step-like signatures associated with different water masses in the region.

Next we classify the temperature and color fields using the same procedure applied to the SAR imagery and then proceed with the fusion problem. The task of fusing information over the same region/feature from three separate sensors raised two problems. The first problem resulted from the differences in repeat cycles of different satellites, as well as cloud cover which limited our data base to only two days, during which all three sensors imaged the same region near-simultaneously. The AVHRR image was taken almost seven hours prior to the ERS-2/SAR pass, while the SeaWIFS pass occurred approximately two hours after the ERS-2/SAR pass. The second problem was the registration of the various images having different spatial resolutions. Instead of registering the various images on a pixel-by-pixel basis, which would have resulted in loss of information for the high-resolution SAR image; we projected the coordinates of the classification labels from the low-resolution imagery onto the geo-referenced SAR image. In Fig. 11 yellow circles represent the positions of step-like features in the ocean-color field, and red circles representing the SST field.

We now turn to the sensor-fusion problem and pose certain hypotheses using declarative and procedural knowledge. For example using a single sensor, ie, a SAR we are able to discriminate between roughness fronts the signatures of which are linked to hydrodynamic processes versus wind stress variations, ie, pulse-shaped or step-like signatures. There are situations, however, in which a single sensor will give ambiguous results due to the similarities of the feature signatures. Such a situation arises with the step-like front observed in Fig 10a. Given only the roughness signature, it is unclear whether the signature is of SST or wind origin and additional physical evidence is required. If we utilize the AVHRR sensor as supplementary evidence and the following set of elements:

$$\text{SST Front: } SSTF = \{p_{1S}, p_{1A}\} \quad \text{and} \quad \text{Wind Front: } WF = \{p_{2S}, p_{2A}\} \tag{3.1}$$

Where:

p_{1S} : probability of having a step-type profile from SAR sensor.
p_{2S} : probability of having a uniform profile from SAR sensor.
p_{1A} : probability of having a step-type profile from AVHRR sensor.
p_{2A} : probability of having a uniform profile from AVHRR sensor.

S_1 and S_2 are the SAR-roughness responses, and A_1 and A_2 are the AVHRR-SST responses respectively, for the two features, the pattern recognition system (Fig. 12) can form a hypothesis based on:

- Rule1: the feature is a SSTF if S_1 and A_1 are both steps.

Or,

- Rule 2: the feature is a WF if S_2 is a step while A_2 is a constant.

In SAR imagery a step-type profile response occurs for both SSTF and WF. Thus with $p_{1S} \geq p_{2S}$ support must be given to both fronts, and one cannot discriminate between the two fronts. So the FOD is

$$m_1(\{\text{WINF, SSTF}\}) = p_{1S} \tag{3.2}$$
$$m_1(\{\theta\}) = 1 - p_{1S} \tag{3.3}$$

When $p_{2S} \geq p_{1S}$ support is given to "other" non-step phenomena (with uniform response) observed in SAR imagery:

$$m_1(\{\text{other}\}) = p_{2S} \tag{3.4}$$
$$m_1(\{\theta\}) = 1 - p_{2S} \tag{3.5}$$

With the addition of the AVHRR sensor if $p_{1A} \geq p_{2A}$, then support is given to SSTF:

$$m_2(\{\text{SSTF}\}) = p_{1A} - p_{2A} \tag{3.6}$$
$$m_2(\{\theta\}) = 1 - p_{1A} + p_{2A} \tag{3.7}$$

Whereas if $p_{2A} \geq p_{1A}$ support is given to WF. However, since it is likely to have other types of phenomena (non-step) in AVHRR, support must also be given to "other":

$$m_2(\{\text{WINF, other}\}) = p_{2A} - p_{1A} \tag{3.8}$$
$$m_2(\{\theta\}) = 1 - p_{2A} + p_{1A} \tag{3.9}$$

As before m_1 and m_2 can be combined using $m = m_1 \oplus m_2$ to arrive at individual mass probabilities using the fused results. The underlying assumption in rule 1 is that time-scales involved in generating SST changes by an atmospheric wind front which in turn would induce roughness changes are generally much longer (several hours) than generating purely wind-driven roughness changes (seconds). Given that there is good spatial correlation between the step-like roughness front and the AVHRR-derived SST front, we can conclude that the step-like roughness front is associated with a SST front. We attribute some of the dislocation in the northwest region of the image where the two fronts begin to diverge (Fig. 11) to advection during the seven hour period.

The other remarkable outcome of the fusion result is (Fig. 11) the near-perfect co-registration of the bright-narrow radar bands (Gaussian-shaped pulse) and step-like changes in the color field, which we suspect to be associated with a salinity front. Similar behaviors have been noted for salinity fronts observed on the continental shelf of the eastern U.S. by [22, 23]. The bright radar signatures are attributed to strong current convergence (driven by density anomalies), and small-scale wave breaking in

the frontal zone. Color anomalies are attributed to demarcation of water masses having different salinities and optical properties. If this behavior appears to be a general feature of salinity fronts, the combination of SAR and SeaWIFS would make a powerful detection tool.

4
Conclusions

In this report we describe a neural-network-based classification system for automatic pattern recognition. The study has yielded the following conclusions:

1. Based on training on idealized shapes, the system is capable of automatically detecting and locating frontal features in satellite remote sensing imagery.
2. Utilizing a template consisting of a series of 1-D profiles provides an efficient alternative to 2-D image-feature detection and processing.
3. Use of declarative knowledge in conjunction with a set of predefined rules provides a means for discriminating between physical processes and ocean features.
4. Working in the framework of geo-referenced data base with either symbolic information or image-derived contours makes the sensor fusion problem more manageable.

The approach presented here is well suited to rapid, accurate and systematic search of features in multi-sensor data. The credibility of the methods, however, requires further testing with expanded data set involving multi-sensor signatures as well as simultaneous in situ observations. Future research should focus on expansion of the number of features/signatures in the knowledge bank, the multi-sensor fusion rules, and the relationships between the rules and real ocean processes.

Acknowledgments

We thank Jane Flatmann from DERA, UK, for providing the SAR imagery, and Orbital Imaging Corp., USA for providing the SeaWIFS imagery. NOAA satellite images were prepared by E.Nacini of SACLANTCEN.

References

1. Duda R.O. and Hart P.E., Pattern classification and scene analysis. New York, Wiley, 1973.

2. Lippman, R.P., An introduction to computing with neural nets. *IEEE ASSP Magazine*, 1987: 4- 22.

3. Jain, A.K., Fundamentals of digital image processing, Prentice Hall, New Jersey, 1989.

4. Liu, A.K., Peng, C.Y. and Chang, S.Y.S., Wavelet analysis of satellite images for coastal watch. *IEEE Journal of Oceanic Engineering*, 22, 1997: 9-17.

5. Kittler, J., M., Hatef, Duin, R.P.W. and Matas, J., On combining classifiers. *IEEE Transactions on Pattern Analysis And Machine Intelligence,* 20, 1998: 226-239.

6. Hansen L.K. and Salamon, P., Neural Network Ensembles. *IEEE Transactions Systems, Man, and Cybernetics*, 12, 1990:993-1001.

7. Cho Sung-Bae and Kim, J.H., Combining multiple neural networks by fuzzy integral for robust classification. *IEEE Transactions on Systems, Man, and Cybernetics*, 25, 1995: 380-384.

8. Xu, L., Krzyzak, A. and Suen, C.Y., Methods of combining multiple classifiers and their applications to handwriting recognition. *IEEE Transactions on Systems, Man, and Cybernetics*, 22, 1992: 418435.

9. Shafer, G., A mathematical theory of evidence. Princeton University Press, 1976.

10. Anzai, Y., Pattern recognition and machine learning. Academic Press, Inc., Boston, 1989.

11. Gould, R.W. and Arnone, R.A., Remote sensing estimates of inherent optical properties in a coastal environment. *Remote Sensing of Environment*, 61, 1997:290-301.

12. Alpers, W., Measurements of mesoscale oceanic and atmospheric phenomena by ERS-1 SAR. *The Radio Science Bulletin*, 275, 1995:14-22.

13. Stewart, R.H., Methods of satellite oceanography. University of California Press, 1985.

14. Askari, F., Geernaert, G.L., Keller, W.C. and Raman, S., Radar imaging of thermal fronts. *International Journal of Remote Sensing*, 14, 1993:275-294.

15. Askari, F., Donato, T.F. and Morrison, J.M., Detection of Oceanic fronts at low grazing angles using an X-band real aperture radar. *Journal of Geophysical Research,* 101, 1996: 20883-20898.

16. Johannessen, J.A., Schuchman, R.A., Johannessen, O.M., Davidson, K.L. and Lyzenga, D.R., SAR imaging of upper ocean circulation features and wind fronts. *Journal of Geophysical Research*, 96, 1991:10,411-10,422.

17. Ng K. and Lippmann, R.P., A comparative study of practical characteristics of neural network and conventional pattern classifiers. Lincoln Laboratory tech report 894, Massachusetts Institute of technology, 1991.

18. Paola J.D. and Schowengerdt, R.A., A review and analysis of back-propagation neural networks for classification of remotely-sensed multi-spectral imagery. *International Journal of Remote Sensing*, 16, 1995: 3033-3058.

19. Renals S. and Rohwer, R., Phoneme classification experiments using Radial Basis Functions. *IEEE Int. Joint Conf. on neural networks*, 1989: 461-467.

20. Bezdek, J.C., Ehrlich, R. and Full, W., The fuzzy c-means clustering algorithm. *Computers and Geosciences*, 10, 1984:191-203.

21. Stage, B., Interpretation and fusion of sonar images using evidential reasoning. SACLANTCEN SM-294, NATO UNCLASSIFIED. La Spezia, Italy, NATO SACLANT Undersea Research Centre, 1995.

22. Marmorino, G.O. and Trump, C.L., A salinity front and current rip near Cape Hatteras, N.C. *Journal of Geophysical Research*, 99, 1994: 7627-7638.

23. Marmorino, G.O., Shen, C.Y., Allan, N., Askari, F., Trizna, D.B., Trump, C.L. and Shay, L.K., An occlude coastal oceanic front. Accepted for publication in *Journal of Geophysical Research*, 1999.

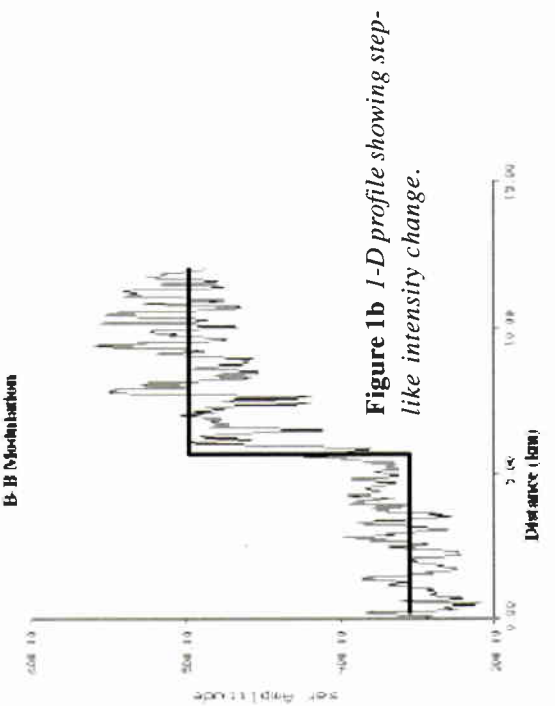

Figure 1b *1-D profile showing step-like intensity change.*

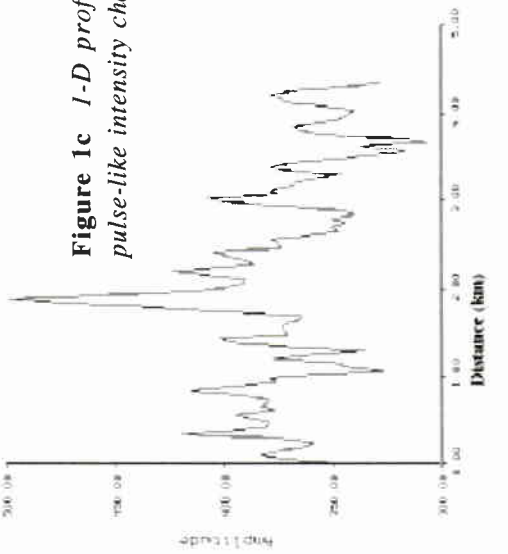

Figure 1c *1-D profile showing pulse-like intensity change.*

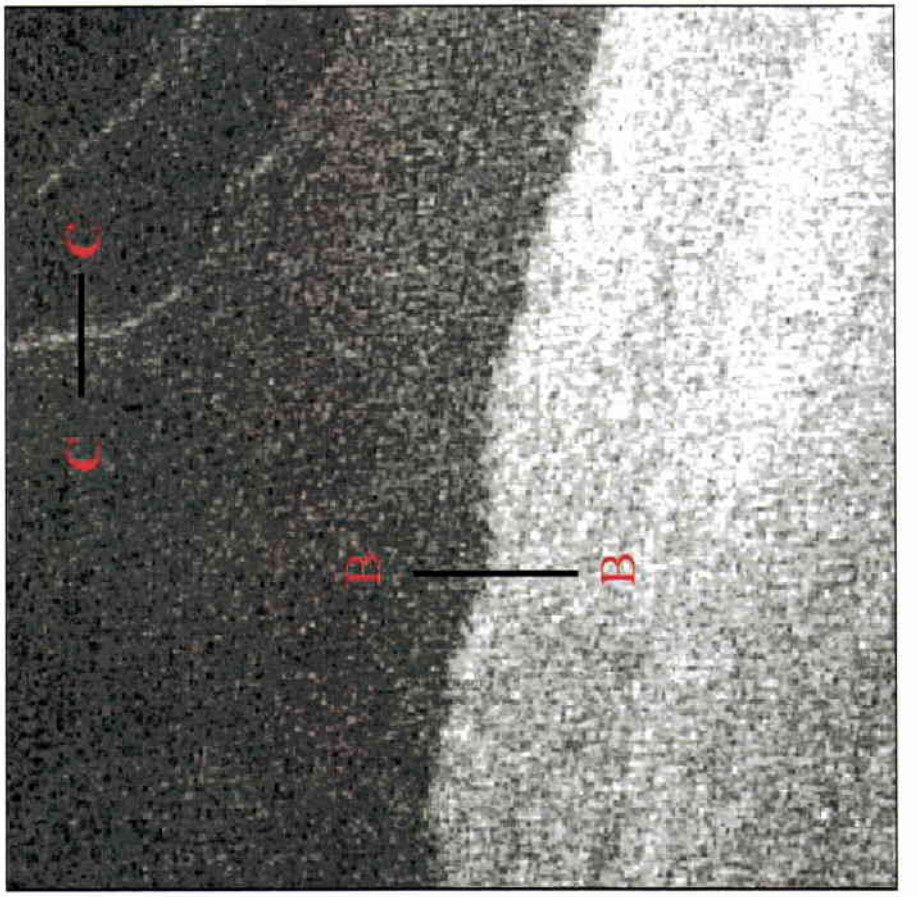

Figure 1a *C-band (5.4 GHz) SAR/ERS2 image with 200x200 pixels (50 m pixel spacing).*

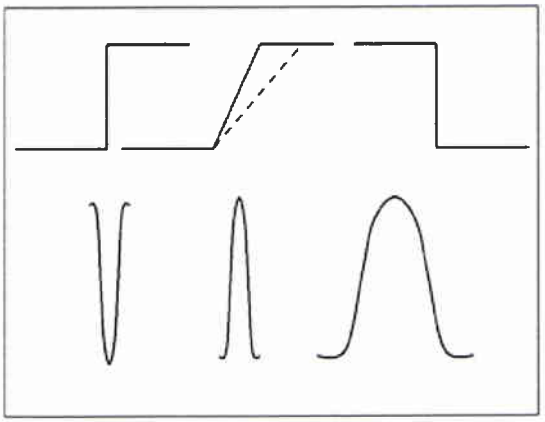

Figure 2 *Idealized training shapes.*

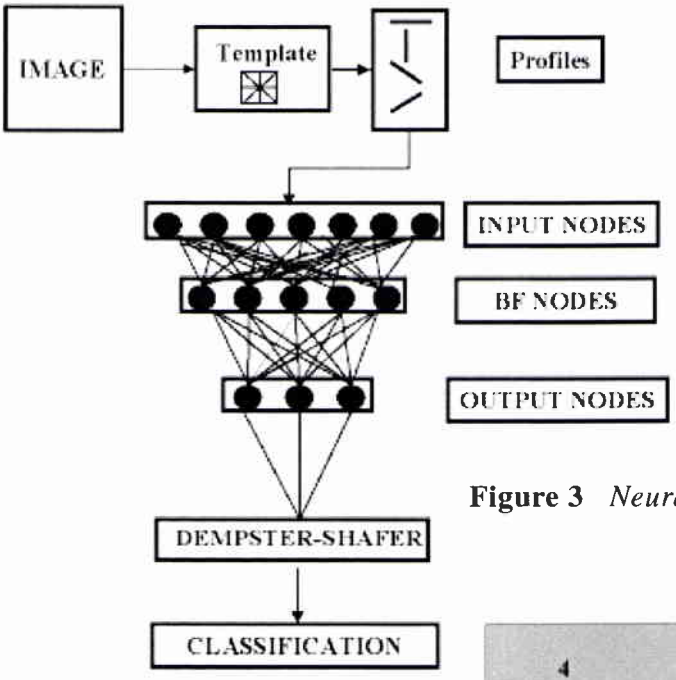

Figure 3 *Neural network architecture.*

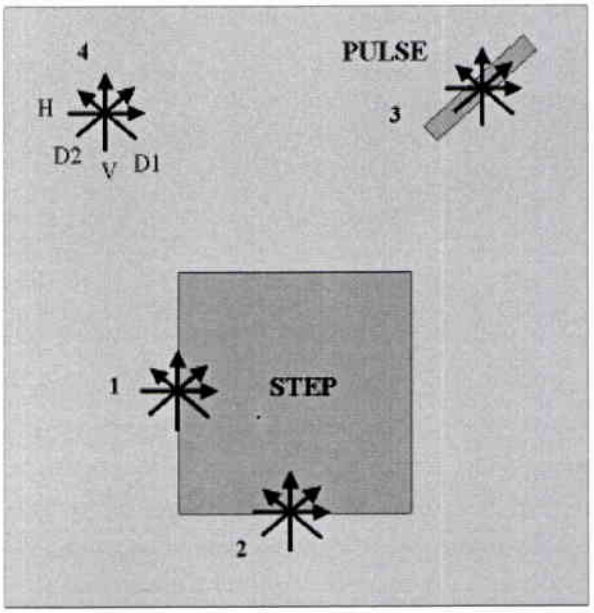

Figure 4 *Idealized features (step and pulse) and the placement of classification template at various locations.*

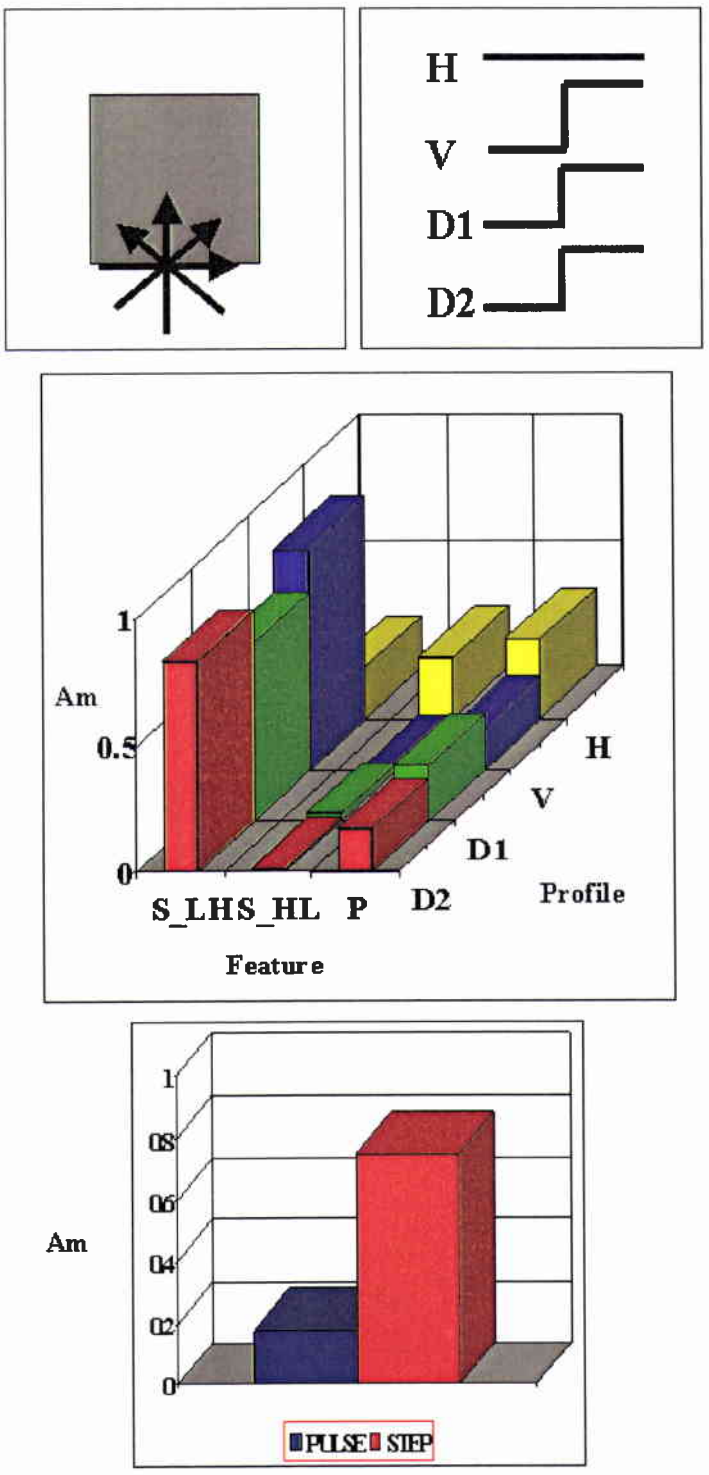

Figure 5 *A) Placement of the template on a horizontal edge, B)the network output matrix, C) the final output from the DS classifier.*

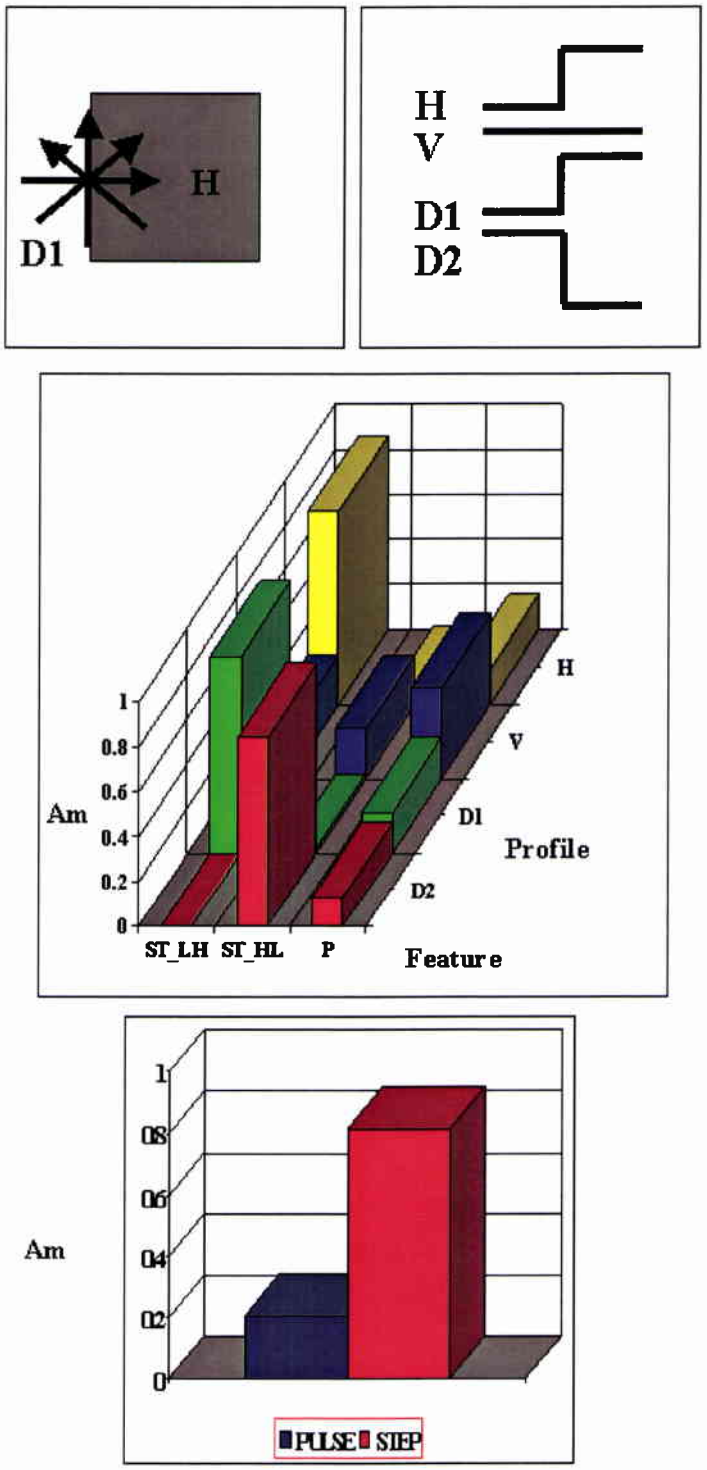

Figure 6 *Same as 6, except for placement of a template on a vertical edge.*

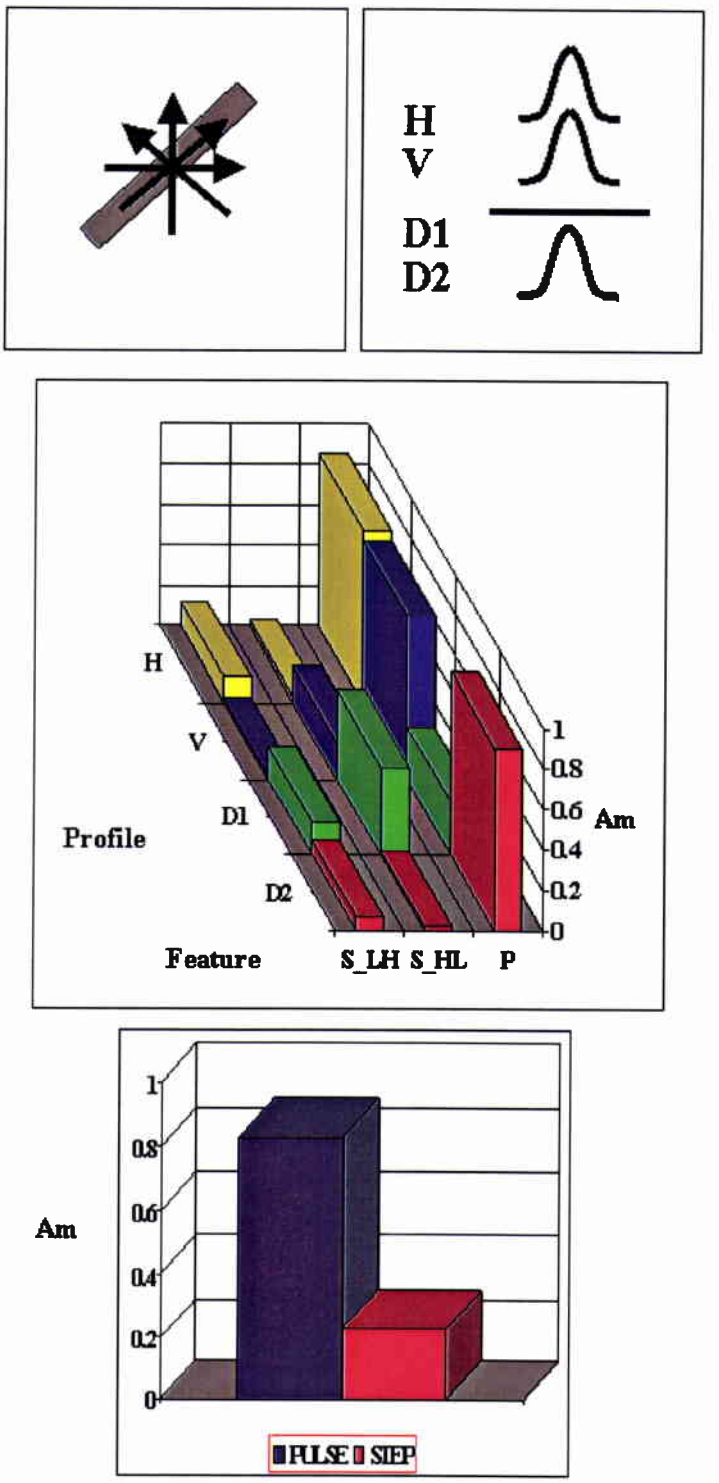

Figure 7 *Same as 6, except for placement of a template on a pulse.*

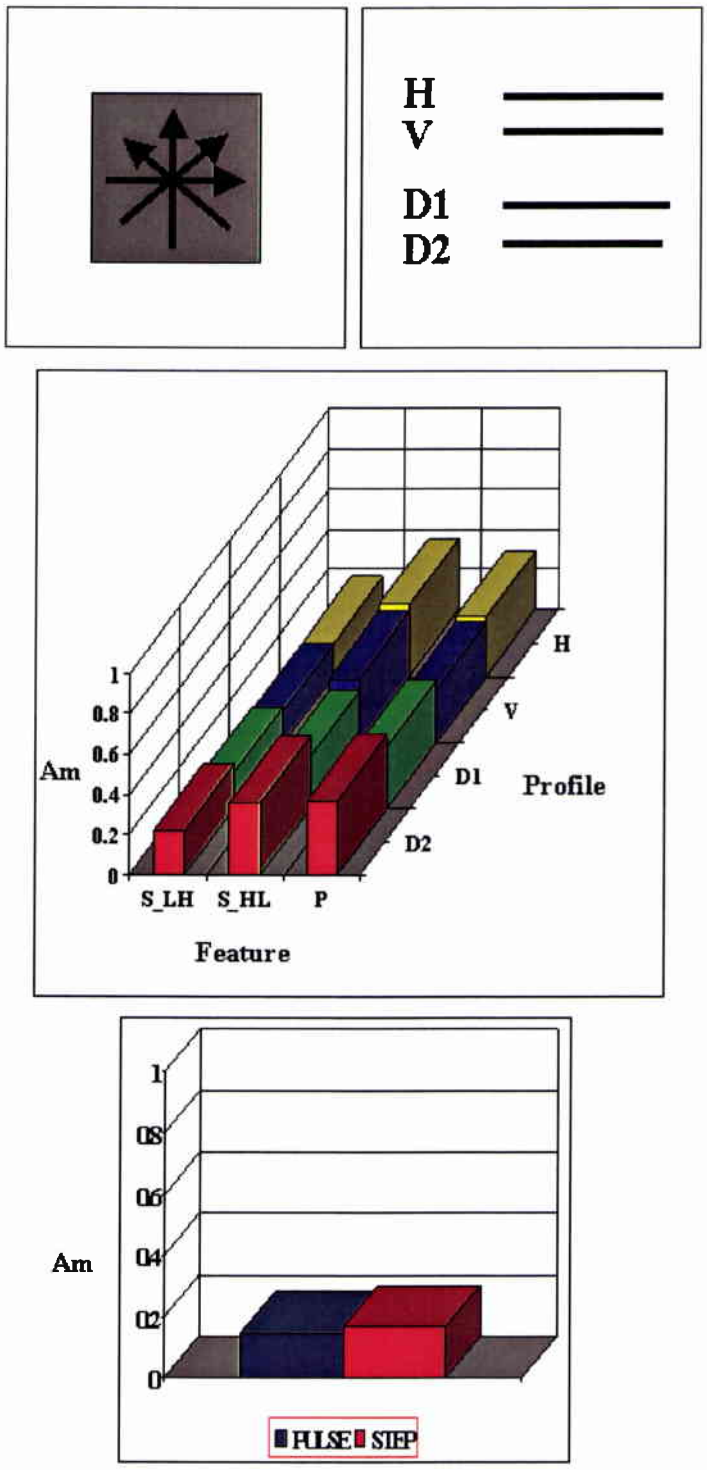

Figure 8 *Same as 6, except for placement of a template on a uniform region.*

Figure 9b *Original SAR image.*

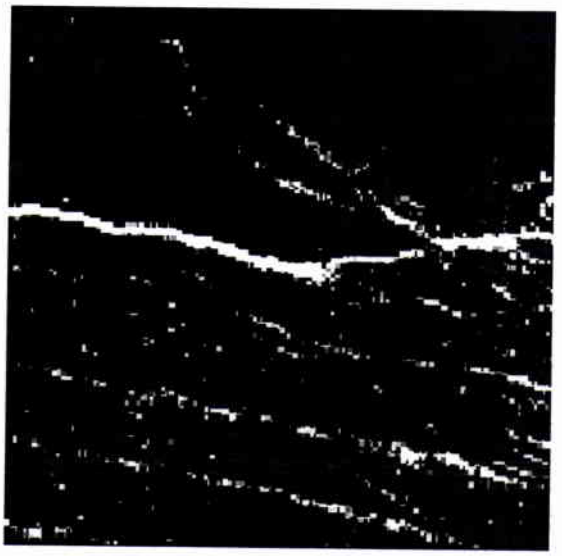

Figure 9b *Classification of step-like features.*

Figure 9c *Classification of pulse-like features.*

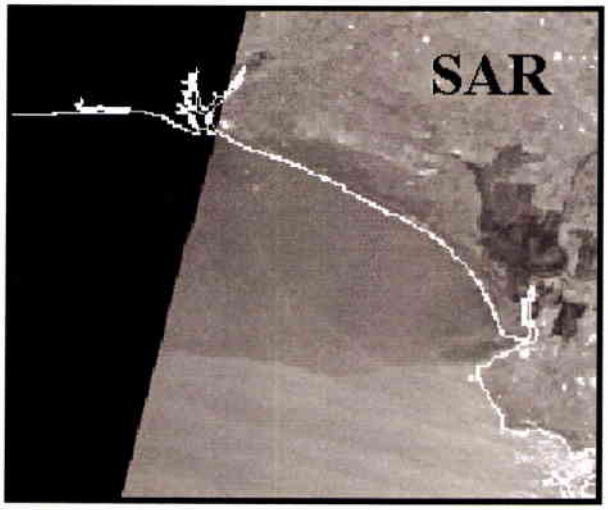

Figure 10a *SAR/ERS2 image with 200x200 pixels (50 m pixel spacing) taken over the Gulf of Cadiz, Spain at 11:08 UT, 14 February 1998.*

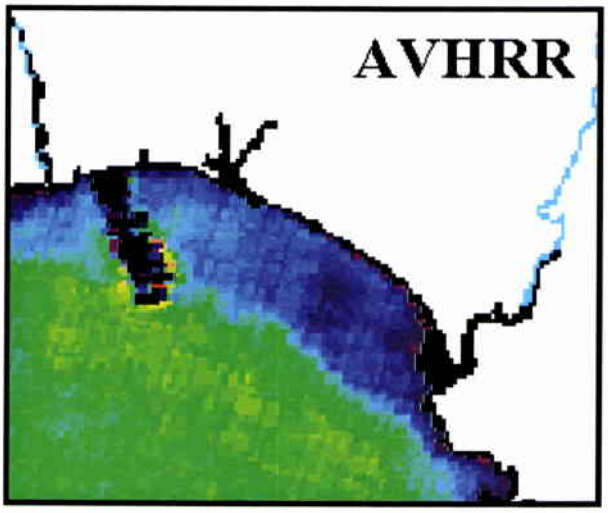

Figure 10b *AVHRR/NOAA-14 image with 1.1 km pixel spacing taken over the Gulf of Cadiz, Spain at 4:01 UT, 14 February 1998.*

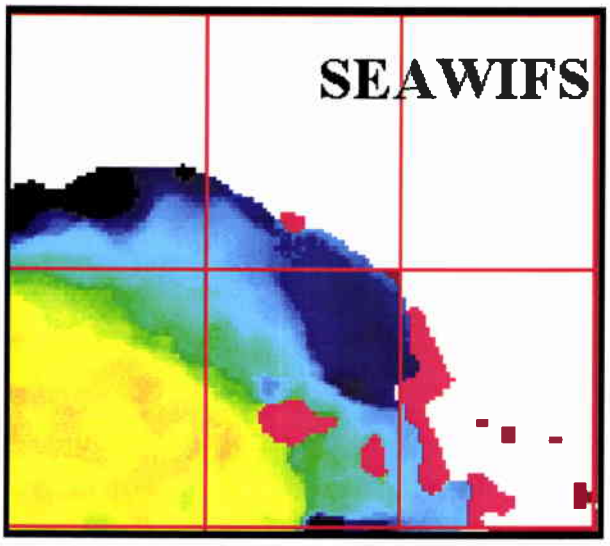

Figure 10c *SeaWIFS/ORBVIEW-2 image with 1.0 km pixel spacing taken over the Gulf of Cadiz, Spain at 13:02 UT, 14 February 1998.*

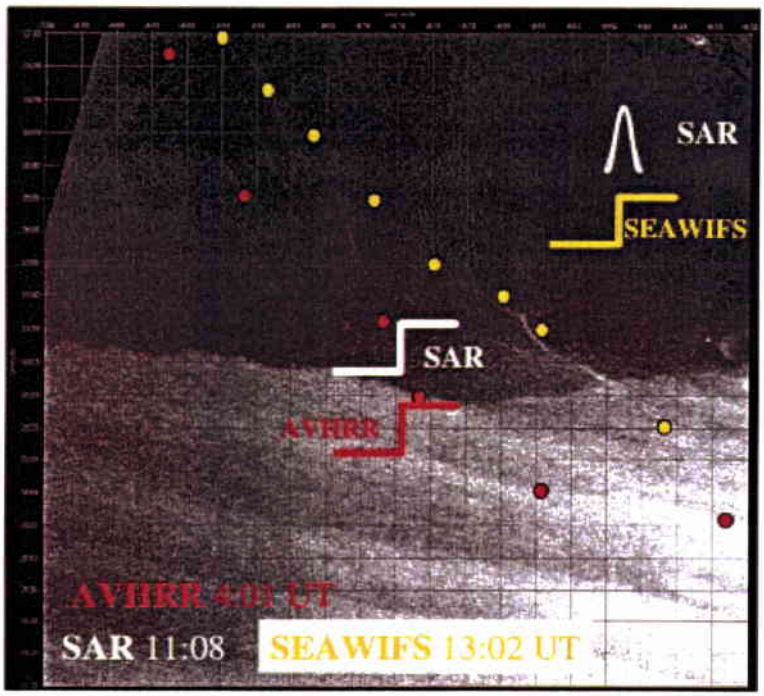

Figure 11 *High resolution SAR image with overlay of classification results from AVHRR and SEAWIFS imagery.*

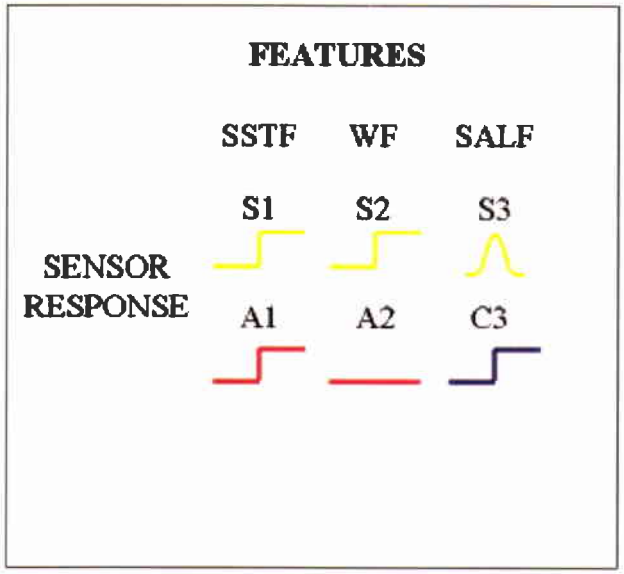

Figure 12 *Sensor fusion architecture.*

Report no. changed (Mar 2006): SR-306-UU

Document Data Sheet

NATO UNCLASSIFIED

Security Classification		Project No.
UNCLASSIFIED		014-1
Document Serial No.	**Date of Issue**	**Total Pages**
SR-306	June 1999	32 pp.

Author(s)

Askari, F., Zerr, B.

Title

A neural-network-fusion architecture for automatic extraction of oceanographic features from satellite remote sensing imagery

Abstract

This report describes an approach for automatic feature detection from fusion of remote sensing imagery using a combination of neural network architecture and the Dempster-Shafer (DS) theory of evidence. Deterministic or idealized shapes are used to characterize surface signatures of oceanic and atmospheric fronts manifested in satellite remote sensing imagery. Raw satellite images are processed by a bank of radial basis function (RBF) neural networks trained on idealized shapes. The final classification results from the fusion of the outputs of the separate RBF. The fusion mechanism is based on DS evidential reasoning theory. The approach is initially tested for detecting different features on a single sensor and extended to classifying features observed by multiple sensors.

Keywords

Malta Plateau - sequence strategy - sea level changes - Quaternary sediments - seismic reflection

Issuing Organization

North Atlantic Treaty Organization
SACLANT Undersea Research Centre
Viale San Bartolomeo 400, 19138 La Spezia, Italy

[From N. America: SACLANTCEN (New York) APO AE 09613]

Tel: +39 0187 527 361
Fax:+39 0187 524 600

E-mail: library@saclantc.nato.int

Initial Distribution for Unclassified SR-306

Ministries of Defence

DND Canada	10
CHOD Denmark	8
DGA France	8
MOD Germany	15
HNDGS Greece	12
MARISTAT Italy	9
MOD (Navy) Netherlands	12
NDRE Norway	10
MOD Portugal	5
MDN Spain	2
TDKK and DNHO Turkey	5
MOD UK	20
ONR USA	34

NATO Commands and Agencies

NAMILCOM	2
SACLANT	3
CINCEASTLANT/ COMNAVNORTHWEST	1
CINCIBERLANT	1
CINCWESTLANT	1
COMASWSTRIKFOR	1
COMSTRIKFLTANT	1
COMSUBACLANT	1
SACLANTREPEUR	1
SACEUR	2
CINCNORTHWEST	1
CINCSOUTH	1
COMEDCENT	1
COMMARAIRMED	1
COMNAVSOUTH	1
COMSTRIKFORSOUTH	1
COMSUBMED	1
NC3A	1
PAT	1

Scientific Committee of National Representatives

SCNR Belgium	1
SCNR Canada	1
SCNR Denmark	1
SCNR Germany	1
SCNR Greece	1
SCNR Italy	1
SCNR Netherlands	2
SCNR Norway	1
SCNR Portugal	1
SCNR Spain	1
SCNR Turkey	1
SCNR UK	1
SCNR USA	2
French Delegate	1
SECGEN Rep. SCNR	1
NAMILCOM Rep. SCNR	1

National Liaison Officers

NLO Canada	1
NLO Denmark	1
NLO Germany	1
NLO Italy	1
NLO Netherlands	1
NLO Spain	1
NLO UK	1
NLO USA	1

Sub-total	199
SACLANTCEN	30
Total	229